

Nonstoichiometric Lithium Iron Phosphate for Lithium-Ion Battery Prepared by Supercritical Hydrothermal Synthesis

Kyoo-Seung Han*

Department of Chemical Engineering and Applied Chemistry, College of Engineering, Chungnam National University, 99 Daehak-ro, Yuseong-gu, Daejeon 34134, Republic of Korea

*Corresponding Author: Kyoo-Seung Han, Department of Chemical Engineering and Applied Chemistry, College of Engineering, Chungnam National University, 99 Daehak-ro, Yuseong-gu, Daejeon 34134, Republic of Korea, Tel: +82-42-821-5897, Email: kshan@cnu.ac.kr

Received Date: August 21, 2023 Accepted Date: September 21, 2023 Published Date: September 23, 2023

Citation: Kyoo-Seung Han (2023) Nonstoichiometric Lithium Iron Phosphate for Lithium-Ion Battery Prepared by Supercritical Hydrothermal Synthesis. J Mater sci Appl 7: 1-13

Abstract

Lithium iron phosphate is a main cathode material for lithium-ion batteries. The battery performance of LiFePO_4 , however, is limited by its small lithium ion diffusivity, which can result in a significant loss of capacity at high currents. To enhance the lithium ion diffusion of LiFePO_4 during the charge and discharge of lithium-ion batteries as well as to control in ease the chemical composition, nonstoichiometric lithium iron phosphate, $\text{Li}_{1-x}\text{FeP}_{1-y}\text{O}_{4-z}$ ($0 < x \leq 0.15$, $0 < y \leq 0.05$, $0 < z \leq 0.2$), consisting in some atomic vacancies is prepared by supercritical hydrothermal synthesis. It is found that the changes in composition and crystal structure greatly influence the capacity and rate performance of nonstoichiometric lithium iron phosphate due to the expansions of direction and space in lithium ion diffusion path.

Keywords: Lithium Iron Phosphate; Supercritical Hydrothermal Synthesis; Lithium-Ion Battery; Cathode Materials

Introduction

Lithium-ion rechargeable batteries are used as power sources of electronic appliances and instruments such as mobile phones, laptop computers, portable power tools, wireless cleaners, etc. Their application field has been broadening to high capacity batteries for electric vehicles and electrical energy storage system. The emergence of high capacity batteries has created a growing demand for improvements in energy storage devices that are cost effective and smaller in size and weight as well as operate for a longer time. In this way, lithium iron phosphate has received considerable attention as a cathode material for lithium-ion battery because of its low price, reasonable specific capacity (169.89 mAh/g), good capacity retention, as well as structural, chemical, electrochemical and thermal stabilization [1-5]. On the other hand, the battery performance of lithium iron phosphate is limited by its small lithium ion diffusivity, which can result in a significant loss of capacity at high currents [3,6-8]. The poor rate capability of LiFePO_4 cathodes makes it difficult to make full use of them in lithium-ion batteries unless modifications are made to improve the slow lithium ion diffusion across the $\text{LiFePO}_4/\text{FePO}_4$ interface.

Stoichiometric lithium iron phosphate, LiFePO_4 is crystallized in the orthorhombic olivine structure with P_{mnb} space group. Figure 1 (a), (b) and (c) respectively illustrate the hexagonal close-packed structures of LiFePO_4 in the view of a -axis, b -axis and c -axis. Those show that lithium

ions form a linear chain of the edge-sharing octahedron in the a -axis, b -axis and c -axis [3,9-11]. Each lithium ion shares an edge with two iron ions and two PO_4 tetrahedrons. As shown in Figure 1, the narrow diffusion paths for lithium ions in the direction of a -axis and c -axis result in its small lithium ion diffusivity. Lithium ions are located close to the sites of O3 oxygen in Figure 1. Therefore, it is expected that when one can prepare O3 oxygen less atmosphere in crystal, the crystal structure of lithium iron phosphate can be changed, and thus higher lithium ion diffusivity can be achieved.

To enhance the lithium ion diffusion of LiFePO_4 during the charge and discharge of the lithium-ion batteries, a nonstoichiometric lithium iron phosphate consisting in some vacancies of O3 oxygen is considered. However, due to the strong P-O bond in PO_4^{3-} , it is difficult to obtain the desired material using common synthetic methods including a solid-state reaction method, molten salt sintering method, sol-gel method, spray pyrolysis method, coprecipitation-sintering method, wet precipitation, and hydrothermal method [2,9,12-15]. In contrast, a nonstoichiometric lithium iron phosphate can be prepared using supercritical hydrothermal synthesis. Moreover, the indirect effect in the improvement of lithium ion conductivity can be expected with shortening lithium ion diffusion routes by making particles ultrafine. In this work, the material characteristics and the battery performances of nanometer sized and nonstoichiometric lithium iron phosphate are presented.

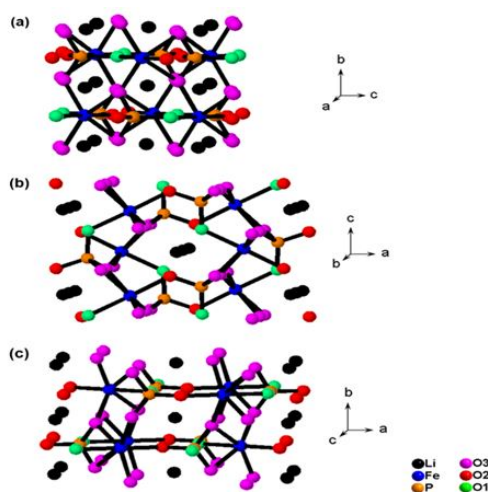


Figure 1: Perspective views of the structure of LiFePO_4 in projection along (a) a -axis, (b) b -axis and (c) c -axis

Experimental

Synthesis of Nonstoichiometric Lithium Iron Phosphate

The preparation procedure of nanometer sized and nonstoichiometric lithium iron phosphate consists of three steps: (1) preparation of three water solutions (FeSO_4 and H_3PO_4 water solution (solution I), NH_4OH and LiOH

water solution (solution II), supercritical water), (2) supercritical hydrothermal reaction and (3) thermal treatment at 700°C during 10 hours for drying, granulation of nanometer sized primary powders and improvement of crystallinity (Figure 2). Various nonstoichiometric lithium iron phosphates are fabricated at the difference in the molar concentration of FeSO_4 , H_3PO_4 , NH_4OH and LiOH solution. The molar concentration of FeSO_4 , H_3PO_4 , NH_4OH and LiOH solution is reported in Table 1.

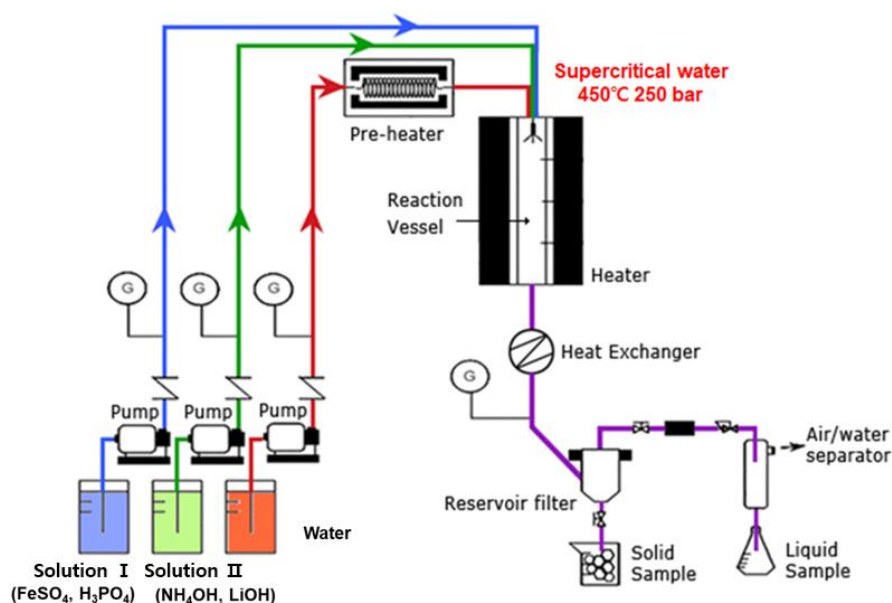


Figure 2: Schematic illustration of supercritical hydrothermal reaction procedure for synthesis of nonstoichiometric lithium iron phosphate

Table 1: Molar concentration of FeSO_4 , H_3PO_4 , NH_4OH and LiOH solution

Product	Molar concentration of water solution (M)				Molar ratio of P/Fe in the product
	FeSO_4	H_3PO_4	LiOH	NH_4OH	
Sample I	1.0	1.0	2.0	1.1	0.960
Sample II	1.0	1.0	2.0	1.3	0.959
Sample III	1.0	1.0	2.0	1.5	0.956
Sample IV	1.0	1.1	2.0	1.1	0.977
Sample V	1.0	1.1	2.0	1.3	0.969
Sample VI	1.0	1.1	2.0	1.5	0.960
Sample VII	1.0	1.2	2.0	1.1	0.985
Sample VIII	1.0	1.2	2.0	1.3	0.980
Sample IX	1.0	1.2	2.0	1.5	0.979
Sample X	1.0	1.0	2.0	2.0	0.940

The solution I is prepared by the mixing of 1.0 M FeSO_4 water solution and H_3PO_4 water solution in a fixed

molar concentration between 1.0 and 1.2. In addition, the solution II is prepared by the mixing of 2.0 M LiOH water solution and NH_4OH water solution in a fixed molar concentration between 1.1 and 2.0. The supercritical water is obtained in the condition of 450 °C and 250 bar.

The supercritical hydrothermal reaction is performed in a continuous reactor with the following conditions: 380 °C, 250 bar, injection of the solution I at the speed of 8.0 g/min, injection of the solution II at the speed of 8.0 g/min, injection of the supercritical water at the speed of 96.0 g/min, reaction time of 7 seconds.

Characterization

An X-ray diffraction pattern of the products was carefully recorded in accordance with the 2θ step of $0.02^\circ / 40$ seconds counting time. In order to improve the atomic positions and the positional quantities of the whole ions in the products, a crystal structure was determined using Rietveld refinement method. In addition, to confirm the molar ratio of Fe and P in the products, inductively coupled plasma atomic emission spectroscopy (ICP-AES) analysis was also required.

Micro-battery test was carried out using a granule

of the sample I (18 μm in diameter) connected to platinum microelectrode (20 μm in diameter) as cathode, lithium foil as anode and a 1 M LiClO_4 solution in ethylene carbonate (EC)/propylene carbonate (PC) (50/50, volumetric %) as electrolyte.

Electrochemical lithium intercalation/deintercalation experiments of the products were realized by charge/discharge of coin type lithium ion batteries using a mixture of the products (90% in weight) with acetylene black (5% in weight) and polyvinylidene fluoride (PVdF, 5% in weight) as cathode, lithium foil as anode and a 1 M LiPF_6 solution in ethylene carbonate (EC)/dimethyl carbonate (DMC) (50/50, volumetric %) as electrolyte.

Results and Discussion

X-ray diffraction profiles both observed and refined patterns for the sample I as well as difference between observed and refined intensities are shown in Figure 3. The measured diffraction pattern overlaps with the calculated diffraction pattern (based on P_{nma} space group) and the difference is represented by the bottommost line. Rietveld refinement is performed by minimizing R_{wp} (weighted pattern R factor), which is the difference between the measured and calculated profiles.

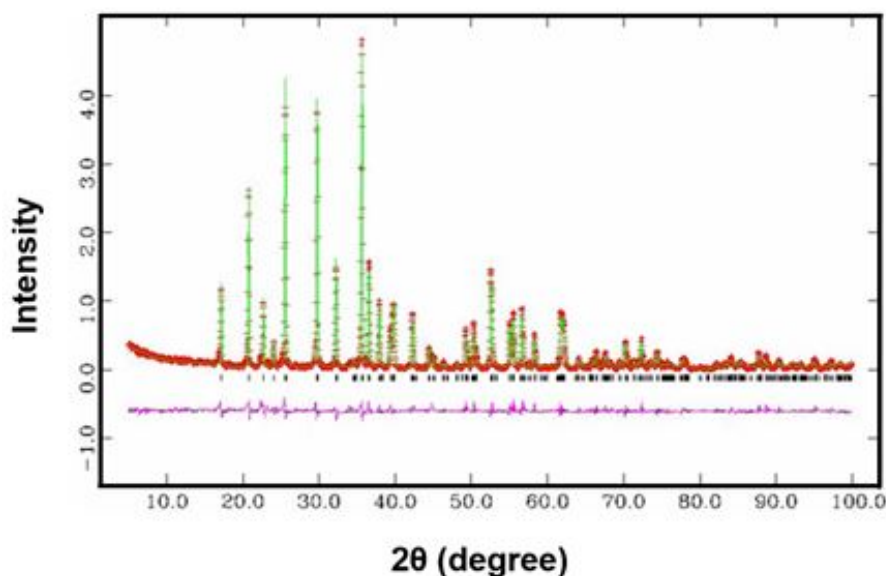


Figure 3: Rietveld refinement of X-ray diffraction patterns for sample I corresponding to $\text{Li}_{0.87}\text{FeP}_{0.96}\text{O}_{3.94}$. Color code: red; collected pattern, green; refined pattern, pink; difference between collected and refined pattern

Table 2: Refined atomic coordinates and quantities for the atoms of the sample I

Site	Atom	Number	x	y	z	Occupancy	Quantity
Li1	Li ⁺	4	0.00000	0.00000	0.00000	0.879	0.869
Fe1	Fe ²⁺	4	0.28220	0.25000	0.97160	1.011	1.000
P1	P ⁵⁺	4	0.09540	0.25000	0.41790	0.970	0.960
O1	O ²⁻	4	0.09460	0.25000	0.74030	1.001	0.990
O2	O ²⁻	4	0.45380	0.25000	0.20560	1.007	0.996
O3	O ²⁻	8	0.16150	0.05210	0.28610	0.987	1.953
R_w	11.62						

The results of Rietveld refinement are considered reliable when R_w obtained using a least squares approach is found to be less than 10. The refined atomic coordinates and quantities are given in Table 2. Regrettably, in this work, the minimized R_w values is 11.62. It might result from less uniform distribution of the atomic vacancies as well as small particle size of the ultrafine powders. Nevertheless, the X-ray diffraction pattern for the sample I is well in-

dexed in the orthorhombic olivine structure with P_{nma} space group. As given in Table 2, the result of the Rietveld refinement demonstrates the presence of atomic vacancies in the sample I and the chemical formula for the sample I of $Li_{0.87}FeP_{0.96}O_{3.94}$. The investigation into the Rietveld refinement of X-ray diffraction patterns for all the samples, $Li_xFeP_{1-y}O_{4-z}$ ($0 < x \leq 0.15$, $0 < y \leq 0.05$, $0 < z \leq 0.2$), will be reported in forthcoming papers.

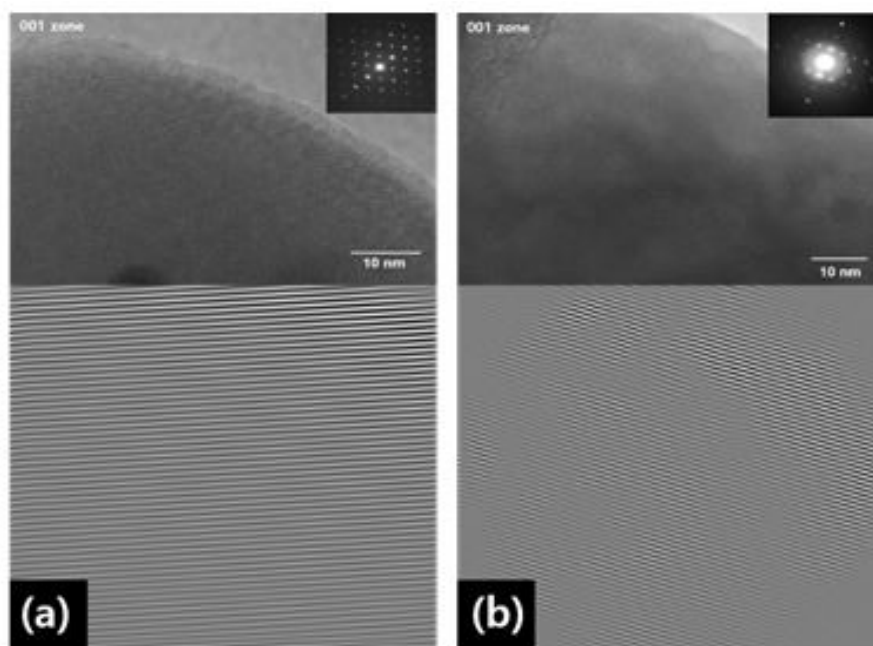


Figure 4: HR-TEM image and SAED pattern, indexing of diffraction patterns and Fourier-filtered image in 001 zone, (a) $LiFePO_4$, (b) $Li_{0.87}FeP_{0.96}O_{3.94}$

Figure 4 (a) and (b) show high-resolution (HR) transmission electron microscopy (TEM) images and selected area electron diffraction (SAED) patterns of a commercial $LiFePO_4$ and the sample I, $Li_{0.87}FeP_{0.96}O_{3.94}$, respectively. The HRTEM results of $LiFePO_4$ demonstrate its highly or-

dered crystal lattices without any dislocations and structural defects [16-18]. However, the Y-type diffraction patterns and the slightly curved diffraction patterns in the HRTEM image as well as the halation in the SAED pattern in Figure 4 (b) indicate that $Li_{0.87}FeP_{0.96}O_{3.94}$ has some atomic vacancies

as point defects that cause a structural deformation [19,20].

The Fourier-transform infrared (FTIR) spectra of the sample I, the sample III, the sample IV, the sample VI and commercial LiFePO_4 are reported in Figure 5 (a), (b), (c), (d) and (e), respectively. It is clear that the FTIR spectra of all the samples exhibit strong similarities. While the vibration frequencies of all the samples and commercial LiFePO_4 in the range of 400 to 700 cm^{-1} are similar, those band shapes are quite different. The bands in the range of 400 to 700 cm^{-1} correspond to bending vibration modes of O-P-O [9,21,22]. In the range of 900 to 1200 cm^{-1} , both the vibra-

tion frequencies and the band shapes between all the samples and commercial LiFePO_4 are changed. The bands in the range of 900 to 1200 cm^{-1} correspond to stretching vibration modes of PO_4 [9,21-25]. Especially, the vibration frequencies of all the samples are moved to higher values compared to those of commercial LiFePO_4 . These changes mean the structural deformation in PO_4 monomer and the reinforcement of P-O band strength due to the atomic vacancies in the samples. In addition, the reinforcement of P-O band strength results in the decrease of P-O bond length and the expansions of direction and space in lithium ion pathway.

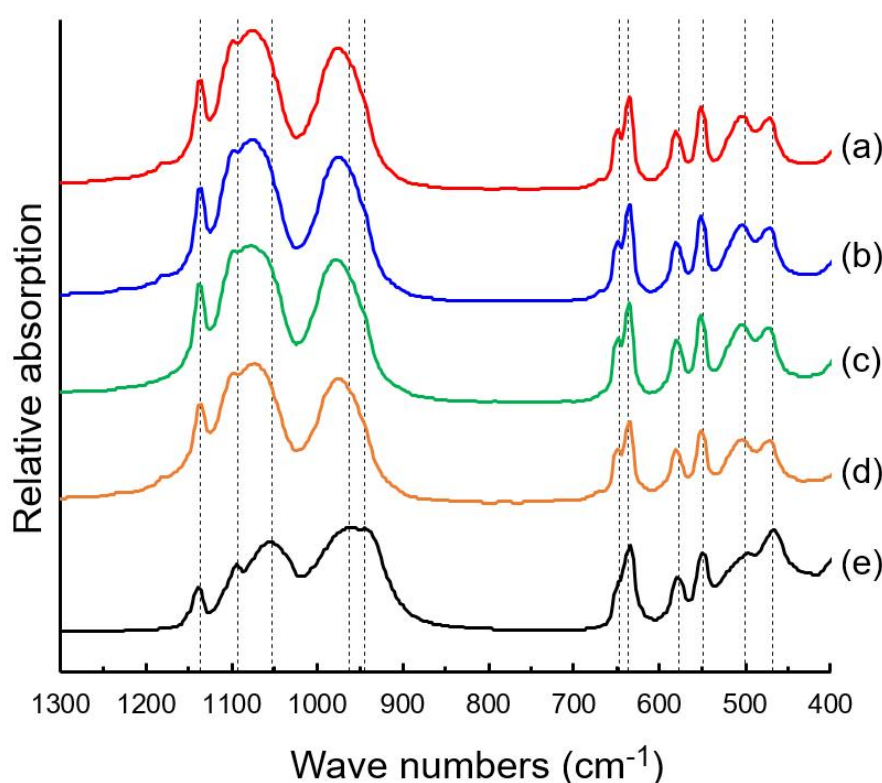


Figure 5: FTIR spectra of (a) sample I, (b) sample III, (c) sample IV, (d) sample VI and (e) commercial LiFePO_4

Scanning electron microscopy (SEM) images in Figure 6 directly shows the spherical granules of nanometer sized $\text{Li}_{0.87}\text{FeP}_{0.96}\text{O}_{3.94}$ powders and also informs of the ap-

proximate sizes of the granule and the primary powder. Figure 6 (a) show the primary powder of $\text{Li}_{0.87}\text{FeP}_{0.96}\text{O}_{3.84}$, and its granules are shown in Figure 6 (b). Mostly the powders are in sphere form.

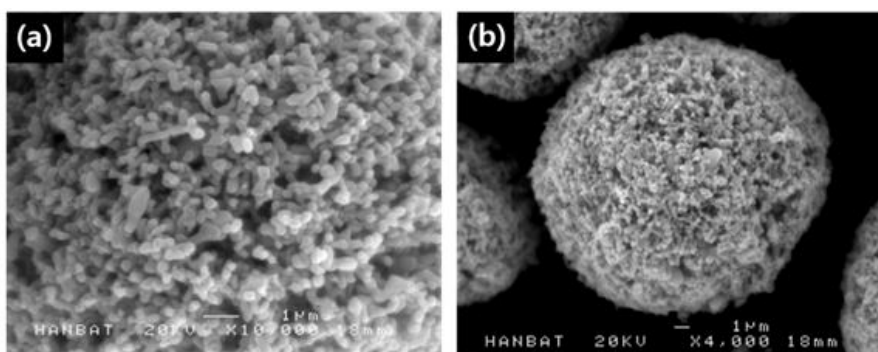


Figure 6: SEM images of $\text{Li}_{0.87}\text{FeP}_{0.96}\text{O}_{3.94}$, (a) the primary powders, (b) the granules

Figure 7 (a) and (b) show the lithium ion diffusion coefficient for $\text{Li}_{0.87-x}\text{FeP}_{0.96}\text{O}_{3.94}$ and $\text{Li}_{1-x}\text{FePO}_4$, respectively. According to x , the highest value of $\text{Li}_{0.87-x}\text{FeP}_{0.96}\text{O}_{3.94}$ was 9.63×10^{-9} and the lowest was 1.01×10^{-9} , while the highest value of $\text{Li}_{1-x}\text{FePO}_4$ was 5.96×10^{-10} and the lowest value was 3.67×10^{-11} . In the same x , the lithium ion diffusion coefficient for $\text{Li}_{0.87-x}\text{FeP}_{0.96}\text{O}_{3.94}$ is 12~27 times high in comparison with that for $\text{Li}_{1-x}\text{FePO}_4$. These differences of lithium ion diffusion mean that the structural change of $\text{Li}_{0.87}\text{FeP}_{0.96}\text{O}_{3.94}$ expands the lithium ion transfer path [26].

Figure 8 (a) and (b) show the Nyquist plots of impedance for $\text{Li}_{0.87}\text{FeP}_{0.96}\text{O}_{3.94}$ and LiFePO_4 , respectively. The real impedance (Z') for $\text{Li}_{0.87}\text{FeP}_{0.96}\text{O}_{3.94}$ is under half the Z' for LiFePO_4 in solid electrolyte interphase, charge transfer electrochemical double layer and mass transport areas.

This difference means the resistance of $\text{Li}_{0.87}\text{FeP}_{0.96}\text{O}_{3.94}$ is smaller than LiFePO_4 at both surface and inner part of powder by reducing amount of oxygen and corresponding structural changes.

The variations of the cell voltage in the range between 2.0 and 4.0 V at 25 °C vs micro-battery capacity for a granule of $\text{Li}_{0.87}\text{FeP}_{0.96}\text{O}_{3.94}$ during discharging under various C-rates are given in Figure 9. Extraordinarily, the discharge capacity at 135 C is 58.7% of the discharge capacity at 1 C, which means that the micro-battery can be fully discharged in 27 seconds (1/135 hour). Existing cellular phones require a charge/discharge rate of 0.5 C. Hybrid electric vehicles require output C-rate of 40 C [3,27]. Unfortunately, the $\text{Li}_{0.87}\text{FeP}_{0.96}\text{O}_{3.94}/\text{Li}$ microbattery is capable of operating up to 20 C.

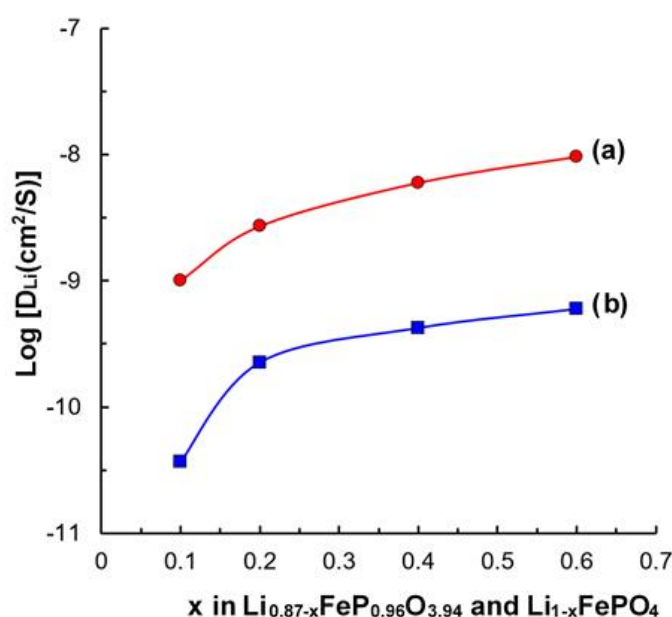


Figure 7: Variation of lithium ion diffusion coefficient vs x for (a) $\text{Li}_{0.87-x}\text{FeP}_{0.96}\text{O}_{3.94}$ and (b) $\text{Li}_{1-x}\text{FePO}_4$

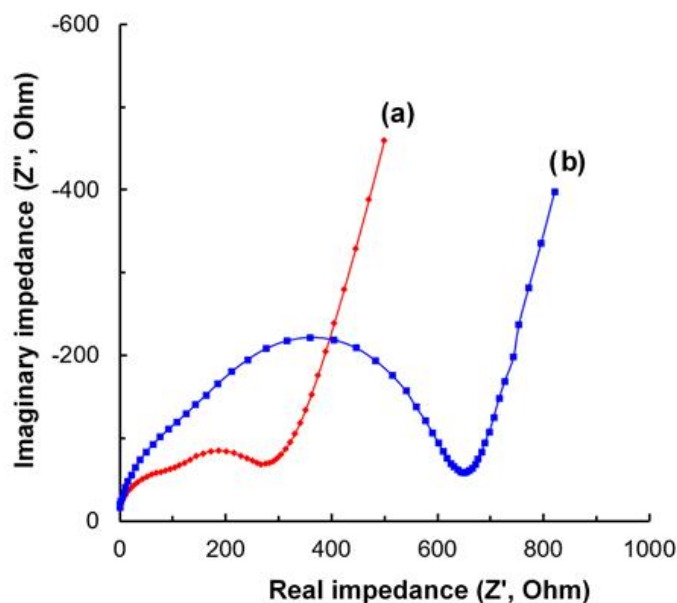


Figure 8: Nyquist plots of impedance for (a) $\text{Li}_{0.87}\text{FeP}_{0.96}\text{O}_{3.94}$ and (b) LiFePO_4

The charge and discharge curves of the $\text{LiFePO}_4//\text{Li}$ cell and the $\text{Li}_{0.87}\text{FeP}_{0.96}\text{O}_{3.94}/\text{Li}$ cell at 0.1 C are shown in Figure 10 (a) and (b), respectively. The $\text{Li}_{0.87}\text{FeP}_{0.96}\text{O}_{3.94}/\text{Li}$ cell exhibits the discharge capacity of 162.58 mAh/g, which is 95.7% of the theoretical capacity of LiFePO_4 . Due to the improved lithium ion mobility and the lower impedance, the $\text{Li}_{0.87}\text{FeP}_{0.96}\text{O}_{3.94}/\text{Li}$ cell has much bet-

ter battery performances such as the nominal voltage drop (gap between charge and discharge potential) and the discharge capacity in comparison with the $\text{LiFePO}_4//\text{Li}$ cell. These results represent that the coulomb efficiency and the energy efficiency of the $\text{Li}_{0.87}\text{FeP}_{0.96}\text{O}_{3.94}/\text{Li}$ cell are higher than those of the $\text{LiFePO}_4//\text{Li}$ cell. Figure 11 shows the capacity retention rate vs the number of cycles of the $\text{Li}_{0.87}\text{FeP}_{0.96}\text{O}_{3.94}/\text{Li}$ cell at 1 C.

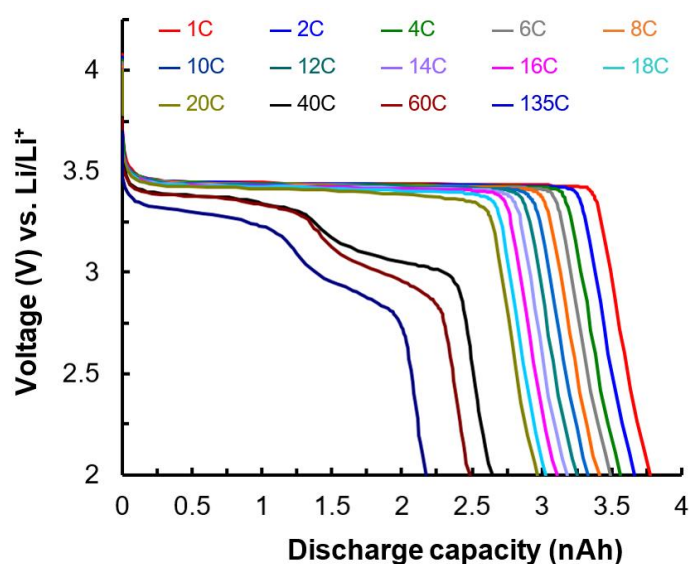


Figure 9: Discharge curves of $\text{Li}_{0.87}\text{FeP}_{0.96}\text{O}_{3.94}/\text{Li}$ micro-battery at various C-rates

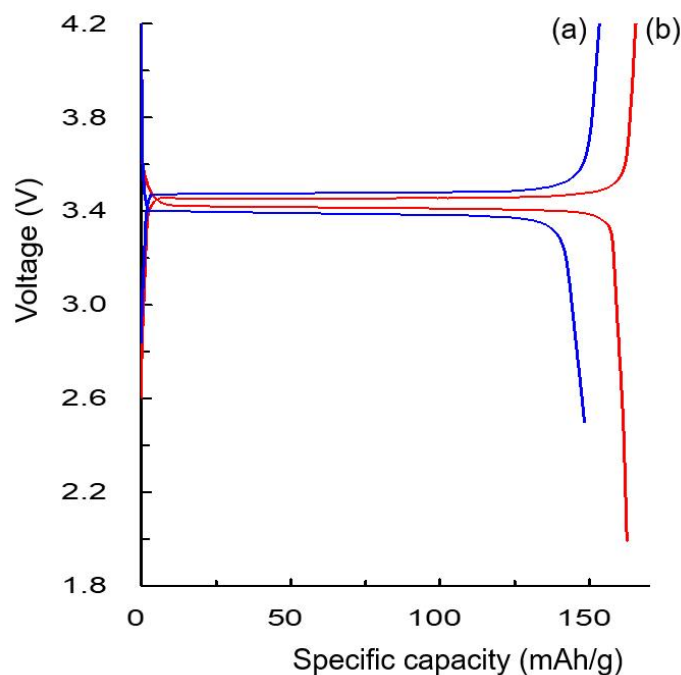


Figure 10: Charge and discharge curves of (a) $\text{LiFePO}_4//\text{Li}$ cell and (b) $\text{Li}_{0.87}\text{FeP}_{0.96}\text{O}_{3.94}//\text{Li}$ cell at 0.1 C

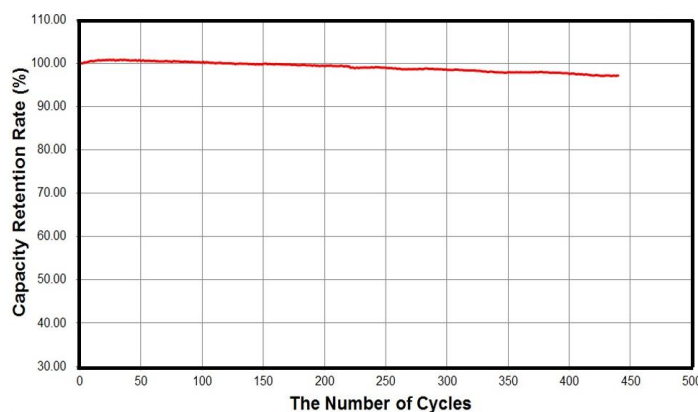


Figure 11: Capacity retention rate vs the number of cycles of $\text{Li}_{0.87}\text{FeP}_{0.96}\text{O}_{3.94}//\text{Li}$ cell at 1 C

In order to find optimum chemical composition of nonstoichiometric lithium iron phosphate, the variation of the specific capacity vs P/Fe molar ratio in $\text{Li}_{1-x}\text{FeP}_{1-y}\text{O}_{4-z}$ ($0 < x \leq 0.15$, $0 < y \leq 0.06$, $0 < z \leq 0.2$) is collected in Figure 12 during the cycles of the $\text{Li}_{1-x}\text{FeP}_{1-y}\text{O}_{4-z}//\text{Li}$ cells. As the P/Fe molar ratio decreases from 1.00 to 0.96, the specific capacity gradually increases. Conversely, as the P/Fe molar ratio decreases from 0.96 to 0.95, the specific capacity gradually decreases. Unfortunately, in the case with a P/Fe molar ratio

of less than 0.95, the specific capacity rapidly decreases. The capacity at P/Fe molar ratio 0.96 was the highest. According to decreasing the P/Fe molar ratio from 1.00 to 0.96, $\text{Li}_{1-x}\text{FeP}_{1-y}\text{O}_{4-z}$ has the gradual widening of the lithium ion diffusion path while maintain its structural stability. However, $\text{Li}_{1-x}\text{FeP}_{1-y}\text{O}_{4-z}$ with a P/Fe molar ratio of less than 0.95 has too many atomic vacancies, which cause the destruction of the structural stability. The structural instability of $\text{Li}_{1-x}\text{FeP}_{1-y}\text{O}_{4-z}$ with a P/Fe molar ratio of less than 0.95 makes an irreversible cycle.

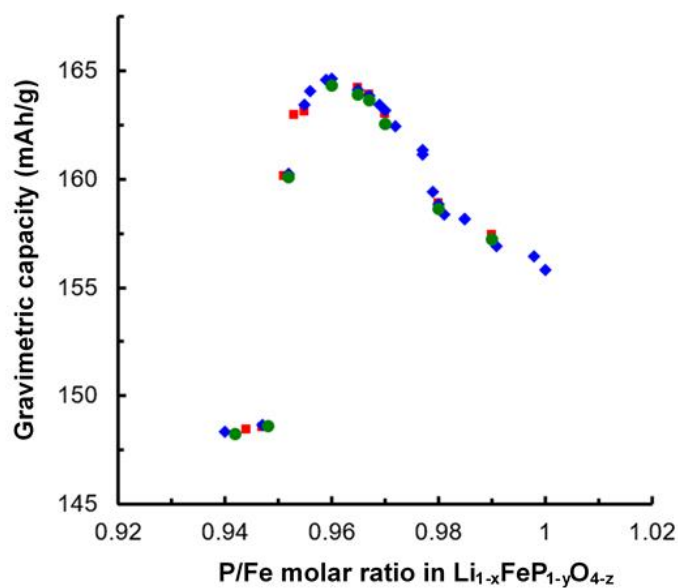


Figure 12: Variation of the specific capacity vs P/Fe molar ratio in $\text{Li}_{1-x}\text{FeP}_{1-y}\text{O}_{4-z}$

Conclusion

To enhance the battery performance of LiFePO_4 , nanometer sized $\text{Li}_{1-x}\text{FeP}_{1-y}\text{O}_{4-z}$ ($0 < x \leq 0.15$, $0 < y \leq 0.05$, $0 < z \leq 0.2$) consisting in some atomic vacancies is fabricated by supercritical hydrothermal synthesis. The $\text{Li}_{0.87}\text{FeP}_{0.96}\text{O}_{3.94}$ //Li micro-battery capacity at 135 C is 58.7% of its discharge capacity at 1 C, which means that the micro-battery can be fully discharged in 27 seconds. Therefore, the

$\text{Li}_{0.87}\text{FeP}_{0.96}\text{O}_{3.94}$ //Li micro-battery has ultrahigh rate capability. It is found that the changes in composition and crystal structure greatly influence the battery capacity and rate performance of $\text{Li}_{1-x}\text{FeP}_{1-y}\text{O}_{4-z}$ due to the expansions of direction and space in lithium ion diffusion path.

Acknowledgement

This work was supported by research fund of Chungnam National University.

References

1. Padhi AK, Nanjundaswamy KS, Goodenough JB (1997) Phospho-olivines as positive electrode materials for rechargeable lithium batteries, *Journal of Electrochemical Society* 144:1188-94.
2. Yang S, Zavalij PY, Whittingham MS (2001) Hydrothermal synthesis of lithium iron phosphate cathodes, *Electrochemistry Communications* 3:505-8.
3. Park JK, Doh CH, Han KS, Hong YS, Kang KS et al. (2012) Principles and applications of lithium secondary batteries, John Wiley & Sons.
4. Jugovic D, Uskokovic D (2009) A review of recent developments in the synthesis produces of lithium iron phosphate powders, *Journal of Power Sources* 190: 538-44.
5. Zhao Q, Zhang S, Li T, Xu C, Yang J et al. (2023) Enhanced electrochemical delithiation of LiFePO₄ in a composite aqueous electrolyte for high performance olivine FePO₄, *Journal of Electrochemical Society* 170: 040521.
6. Chung SY, Bloking JT, Chiang YM (2002) Electronically conductive phospho-olivines as lithium storage electrodes, *Nature Materials* 1: 123-8.
7. Prosini PP, Lisi M, Zane D, Pasquali M (2002) Determination of the chemical diffusion coefficient of lithium in LiFePO₄, *Solid State Ionics* 148: 45-51.
8. Amin R, Balaya P, Maier J (2007) Anisotropy of electronic and ionic transport in LiFePO₄ single crystals. *Electrochemical and Solid-State Letters* 10: 13-6.
9. Ait Salah A, Jozwiak P, Garbarczyk J, Benkhouja K, Zaghbi K et al. (2005) Local structure and redox energies of lithium phosphates with olivine- and Nasicon-like structures, *Journal of Power Sources* 140: 370-5.
10. Kobayashi S, Kuwabara A, Fisher CAJ, Ukyo Y, Ikuhara Y (2018) Microscopic mechanism of biphasic interface relaxation in lithium iron phosphate after delithiation, *Nature Communications* 9: 1-10.
11. Yang S, Song Y, Zavalij PY, Whittingham MS (2002) Reactivity, stability and electrochemical behavior of lithium iron phosphates, *Electrochemistry communications* 4: 239-44.
12. Kim JK, Choi JW, Chauhan GS, Ahn JH, Hwang GC et al. (2008) Enhancement of electrochemical performance of lithium iron phosphate by controlled sol-gel synthesis, *Electrochimica Acta* 53: 8258-64.
13. Ni JF, Zhou HH, Chen JT, Zhang XX (2007) Molten salt synthesis and electrochemical properties of spherical LiFePO₄ particles, *Materials Letters* 61: 1260-4.
14. Wang GX, Bewlay SL, Konstantinov K, Liu HK, Dou SX, Ahn JH (2004) Physical and electrochemical properties of doped lithium iron phosphate electrodes, *Electrochimica Acta* 50: 443-7.
15. Xie H, Zhou Z (2006) Physical and electrochemical properties of mix-doped lithium iron phosphate as cathode material for lithium ion battery, *Electrochimica Acta* 51: 2063-7.
16. Chen G, Song X, Richardson TJ (2006) Electron microscopy study of the LiFePO₄ to FePO₄ phase transition, *Electrochemical and Solid State Letters* 9: 295-8.
17. Zhao Q, Zhang Y, Meng Y, Wang Y, Ou J et al. (2017) Phytic acid derived LiFePO₄ beyond theoretical capacity as high-energy density cathode for lithium ion battery, *Nano Energy* 34: 408-20.
18. Teng F, Santhanagopalan S, Lemmens R, Geng X, Patel P, Meng DD (2010) In situ growth LiFePO₄ nanorod arrays under hydrothermal condition, *Solid State Sciences* 12: 952-5.
19. Kiely CJ, Pond RC, Kenshole G, Rockett A (1991) A TEM study of the crystallography and defect structures of single-crystal and polycrystalline copper indium diselenide, *Philosophical Magazine A-Physics of Condensed Matter Structure Defects and Mechanical Properties* 63: 1249-73.
20. Aidhy DS, Lu C, Jin K, Bei H, Zhang Y et al. (2015) Point defect evolution in Ni, NiFe and NiCr alloys from atomistic simulations and irradiation experiments, *Acta Materialia* 99: 69-76.
21. Burba CM, Frech R (2004) Raman and FTIR spectro-

copric study of Li_xFePO_4 ($0 \leq x \leq 1$), *Journal of the Electrochemical Society* 151: 1032-8.

22. Ornek A, Bulut E, Ozacar M (2014) The chemical, physical and electrochemical effects of carbon sources on the nano-scale LiFePO_4 cathode surface, *Ceramics International* 40: 15727-36.

23. Brochu F, Guerfi A, Trottier J, Kopec M, Mauger A et al. (2012) Structure and electrochemistry of scaling nano C- LiFePO_4 synthesized by hydrothermal route: complexing agent effect, *Journal of Power Sources* 214:1-6.

24. Miao C, Bai P, Jiang Q, Sun S, Wang X (2014) A novel synthesis and characterization of LiFePO_4 and LiFePO_4/C as a cathode material for lithium-ion battery, *Journal of Pow-*

er Sources 246:232-8.

25. Jozwiak P, Garbarczyk JE, Wasiucionek M, Gorzkowska I, Gendron F et al. (2008) DTA, FTIR and impedance spectroscopy studies on lithium-iron-phosphate glasses with olivine-like local structure, *Solid State Ionics* 179: 46-50.

26. Satyavani TVSL, Ramya Kiran B, Rajesh Kumar V, Srinivas Kumar A, Naidu SV (2016) Effect of particle size on dc conductivity, activation energy and diffusion coefficient of lithium iron phosphate in Li-ion cells, *Engineering Science and Technology an International Journal* 19: 40-4.

27. Nelson P, Amine K, Rousseau A, Yomoto H (2007) presented at Proceedings from the 23rd Electric Vehicle Symposium.

Submit your manuscript to a JScholar journal and benefit from:

- ¶ Convenient online submission
- ¶ Rigorous peer review
- ¶ Immediate publication on acceptance
- ¶ Open access: articles freely available online
- ¶ High visibility within the field
- ¶ Better discount for your subsequent articles

Submit your manuscript at
<http://www.jscholaronline.org/submit-manuscript.php>